International Journal of Nanomedicine

Dovepress
open access to scientific and medical research

Open Access Full Text Article

ORIGINAL RESEARCH

Vancomycin-Loaded in situ Gelled Hydrogel as an Antibacterial System for Enhancing Repair of Infected Bone Defects

Shouye Sun[1], Qian Wang[2], Bin Zhang[3], Yutao Cui[1], Xinghui Si[4], Gan Wang[1], Jingwei Wang[1], Hang Xu[1], Baoming Yuan[1], Chuangang Peng[1]

[1]Orthopaedic Medical Center, The Second Hospital of Jilin University, Changchun, People's Republic of China; [2]Department of Otolaryngology, The First Hospital of Jilin University, Changchun, People's Republic of China; [3]Department of Spinal Surgery, The 964th Hospital of PLA Joint Logistic Support Force, Changchun, People's Republic of China; [4]Changchun Institute of Applied Chemistry, Chinese Academy of Sciences, Changchun, People's Republic of China

Correspondence: Baoming Yuan, Orthopaedic Medical Center, The Second Hospital of Jilin University, Changchun, 130041, People's Republic of China, Email yuanbm@jlu.edu.cn

Purpose: During treatment of infected bone defects, control of infection is necessary for effective bone repair, and hence controlled topical application of antibiotics is required in clinical practice. In this study, a biodegradable drug delivery system with in situ gelation at the site of infection was prepared by integrating vancomycin into a polyethylene glycol/oxidized dextran (PEG/ODEX) hydrogel matrix.

Methods: In this work, PEG/ODEX hydrogels were prepared by Schiff base reaction, and vancomycin was loaded into them to construct a drug delivery system with controllable release and degradability. We first examined the microstructure, degradation time and drug release of the hydrogels. Then we verified the biocompatibility and in vitro ability of the release system. Finally, we used a rat infected bone defect model for further experiments.

Results: The results showed that this antibacterial system could be completely biodegradable in vivo for 56 days, and its degradation products did not cause specific inflammatory response. The cumulative release of vancomycin from the antibacterial system was 58.3% ± 3.8% at 14 days and 78.4% ± 3.2% at 35 days. The concentration of vancomycin in the surrounding environment was about 1.2 mg/mL, which can effectively remove bacteria. Further studies in vivo showed that the antibacterial system cleared the infection and accelerated repair of infected bone defects in the femur of rats. There was no infection in rats after 8 weeks of treatment. The 3D image analysis of the experimental group showed that the bone volume fraction (BV/TV) was 1.39-fold higher ($p < 0.001$), the trabecular number (Tb.N) was 1.31-fold higher ($p < 0.05$), and the trabecular separation (Tb.Sp) was 0.58-fold higher than those of the control group ($p < 0.01$).

Conclusion: In summary, this study clearly demonstrates that a clinical strategy based on biological materials can provide an innovative and effective approach to treatment of infected bone defects.

Keywords: infected bone defects, drug delivery system, hydrogel, vancomycin

Introduction

Treatment of infected bone defects caused by open fractures or replacement of prostheses has always been a challenge in orthopaedics.[1] Infection severely impairs osteogenesis, leading to complications, such as osteomyelitis and infected non-union.[2,3] Infection causes a persistent state of excessive local inflammation that impairs osteogenic differentiation and promotes bone resorption.[4] On the other hand, pathogens can directly inhibit bone repair by damaging the extracellular matrix and infecting osteoblast.[5] The standard treatment regimen comprises antimicrobial therapy and bone reconstruction, with antimicrobial intervention being the primary objective.[6] Bone reconstruction can only commence once the infection is effectively controlled. Currently, common treatment methods in the clinic include debridement of the infection site, systemic administration of antibiotics, and implantation of antibiotic-loaded bone cement.[7] Bone cement,

Received: 20 November 2023
Accepted: 19 March 2024
Published: 11 October 2024

as a targeted drug delivery method, usually has advantages over systemic treatments requiring high doses of antibiotics, and can easily lead to drug resistance.[8] Poly (methyl methacrylate) (PMMA) is the main material used in bone cement.[9,10] However, studies have shown that antibiotics embedded in the PMMA matrix may be suddenly or only partially (~10%) released in vivo.[11,12] This cannot ensure a sustained effective concentration of antibiotics at the lesion site and may stimulate antibiotic resistance. Furthermore, sudden release of antibiotics impairs osteoblast function.[13] In addition, non-biodegradable bone cement forms a biofilm in the body, which favors bacterial proliferation and increases the risk of secondary infection. Therefore, additional surgery is needed to remove the bone cement, causing pain and increasing the economic burden on patients.[14] Therefore, development of a new, biodegradable, and stable local antibiotic delivery system would be of great significance.

In recent years, various antibiotic delivery systems have been developed and successfully applied to the treatment of infected bone defects.[15,16] Hydrogels represent a suitable drug delivery system due to their well-developed 3D network structure, which is conducive to drug loading.[17] The interconnected porous structure of hydrogels facilitates drug diffusion. Moreover, the excellent injectability and plasticity of hydrogels facilitate transplantation into the infected bone defects, enhancing localized therapeutic effects. Additionally, the hydrophilic nature of hydrogels provides a favorable microenvironment for local tissues and they exhibit good affinity with both tissues and cells.[18,19] However, the rapid swelling and degradation of certain hydrogels can lead to localized explosive release of antibiotics over a short period.

PEG is a hydrophilic polymer that has found wide-ranging applications in the field of biomedicine as a component of hydrogels and drug delivery systems.[20] This is due to several favorable characteristics, including non-toxicity, non-immunogenicity, excellent bio-compatibility, and resistance to protein adsorption.[21,22] PEG possesses multiple reactive end groups that provide binding sites for various drugs and materials. The swelling rate and mechanical strength of PEG-based hydrogels can be controlled by altering the molecular weight and concentration of PEG.[23] ODEX is a biodegradable material used in a variety of applications as it can be metabolized and degraded by human tissues.[24] The aldehyde end groups of ODEX can undergo Schiff base reactions with aminated PEG, resulting in the cross-linking and formation of stable hydrogel materials. Compared to chemical crosslinkers, Schiff base reactions are non-cytotoxic and do not require additional crosslinking agents such as initiators or light sources.[25,26] Additionally, the resulting hydrogel exhibits enhanced stability, thereby extending the release period and minimizing the potential for explosive release. The acetaldehyde group in ODEX can form a Schiff's base bond with the amine group on the tissue surface to achieve high adhesion to the tissue.[27] Moreover, the degradation and injectability of the hydrogel can be tuned by adjusting the proportions and concentrations of the two materials. Zhou et al[28] firstly constructed a multi-functional hydrogel system through incorporating PEG-functionalized CuS nanoparticles with surface amino groups into a ODEX and two-arm PEG-NH_2. These hydrogels displayed excellent self-healing and good biocompatibility for application. However, CU^{2+} will be released from the composite hydrogel in a short time. Experimental results showed that different types of multi-arm PEG-NH_2, the oxidation degree of ODEX and the mass ratio of multi-arm PEG-NH_2/ODEX had profound effects on the degradation time and drug release of implants.[29]

In this study, we have developed a controlled and biodegradable vancomycin delivery system (Van/Gel) by incorporating the antibiotic vancomycin, commonly used for treating infectious bone defects, into a PEG/ODEX hydrogel matrix (Scheme 1). The physicochemical properties and antibiotic release profiles of the system were initially investigated. Subsequently, the cellular compatibility and antibacterial performance of the system were evaluated in vitro. Finally, an infectious bone defect model was established to study the in vivo therapeutic efficacy of the antibiotic system.

Materials and Methods

Materials

Dextran was purchased from TCI Co., Ltd. (Shanghai, China), Four-arm PEG-NH_2 was purchased from Beijing J&K Co., Ltd. Dulbecco's Modified Eagle's Medium (high glucose), penicillin/streptomycin, and fetal bovine serum were supplied by Gibco Life Technologies (CA, USA). Mouse embryo osteoblast precursor (MC3T3-E1; CRL-2593; ATCC) cells were purchased from Cellcook (Guangzhou, China). A Cell Counting Kit-8 (CCK-8) assay and calcein-AM-PI

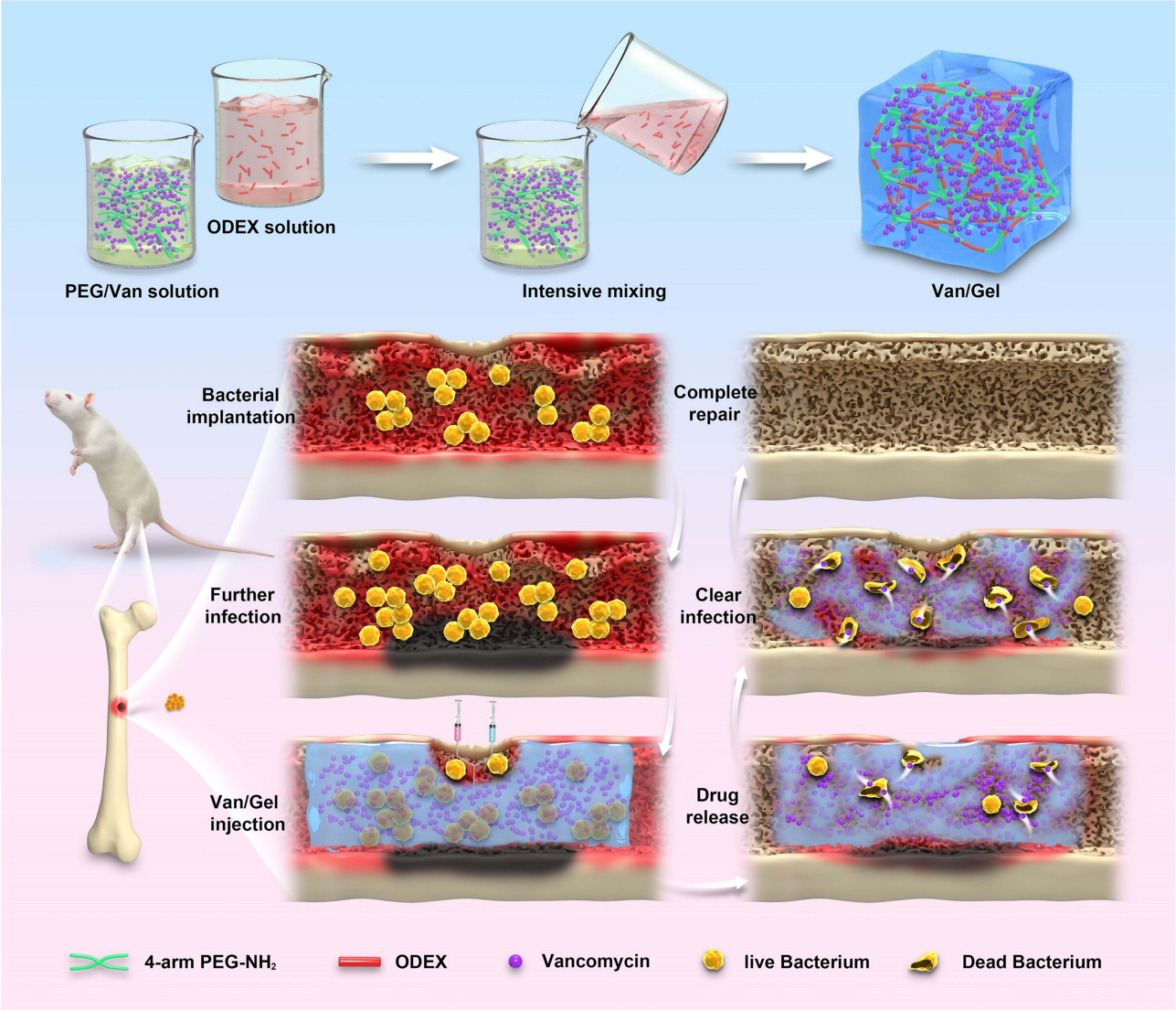

Scheme 1 Preparation of polyethylene glycol/oxidized dextran (PEG/ODEX) hydrogels and repair of infected bone defects in rats.

staining kit were purchased from Invigentech (Irvine, CA, USA). A Live/Dead Cell Staining Kit, Live/Dead Bacterial Staining Kit and Bacterial Viability Assay Kit were purchased from Bestbio (Shanghai, China). 4% paraformaldehyde, DAPI solution, TRITC-phalloidin were purchased from Solarbio (Beijing, China).

Synthesis of ODEX

First, dextran (2.0 g, 12.3 mmol glucose unit) was placed in a 100 mL dry flask, and dextran was completely dissolved in distilled water by continuous stirring at room temperature. Then, sodium periodate (792.0 mg, 3.7 mmol) was added and stirred at room temperature for another 24 hours. Next, the samples were dialyzed with deionized water (MWCO 3500Da) for 3 days. Finally, the liquid obtained from dialysis was placed in cell culture dishes and pre-frozen at −80 °C in a refrigerator for 24 hours. Subsequently, the uniformly prefrozen samples were loaded into the freezing chamber of a freeze dryer. Following sealing, the vacuum pump was activated to eliminate moisture through the process of sublimation. The resultant ODEX was stored in a desiccator.

Preparation of the Van/Gel

The hydrogels were fabricated by mixing four-arm PEG-NH_2 and ODEX through the formation of Schiff base. A PBS solution of vancomycin at a final concentration of 50 mg/mL was first prepared. PEG and ODEX were dissolved into vancomycin solution at a concentration of 10%, respectively. The Van/Gel were then produced by mixing the two solutions at a ratio of 2: 1. The method of preparing PEG/ODEX hydrogels was the same as described above, except that PBS did not contain vancomycin.

Characterization of PEG/ODEX Hydrogels

Scanning Electron Microscopy (SEM)

The structural characteristics of PEG/ODEX hydrogels were studied by Cryo-SEM. Initially, the hydrogels were carefully applied onto a sample stage fixed to the Cryo-SEM apparatus using a pipette. Subsequently, the sample underwent rapid freezing in a liquid nitrogen slush for a duration of 30s. Following the freezing process, the sample was transferred to a pre-cooled preparation chamber at −140 °C under vacuum conditions for controlled fracturing. Subsequent to sublimation at −90 °C for a period of 15 minutes, a platinum layer with an approximate thickness of 5 nm was deposited onto the fractured surface through sputtering. Ultimately, the meticulously prepared sample was introduced into the pre-cooled Zeiss Sigma300 electron microscope set at −140 °C for meticulous observation and imaging. At the same time, we observed the elemental composition of hydrogels by using an energy disposable spectroscope (EDS).

Infrared Spectrum

The synthesized hydrogels were analyzed using an infrared spectrometer (THERMO FISHER NICOLET 6700). The infrared absorption spectra of the sample were obtained by directly placing a small amount of the test sample above a diamond crystal using the point-to-point sampling technique. The OMNIC sampler was tightened with appropriate pressure, and the infrared beam underwent attenuated total internal reflection within the crystal. The infrared absorption spectrum of the sample provided structural information about its organic components.

Rheological Behavior

Rheological experiments were performed on a Physica MCR 301 Rheometer (Anton Paar). The mixture of 10wt% ODEX (100 μL) and 10wt% four-arm PEG-NH_2 (200 μL) was placed between parallel plates of 25 mm diameter and with a gap of 0.3 mm at 37 °C. A frequency of 1 Hz and strain of 1% yielded a linear viscoelastic response. The storage modulus (G') and loss modulus (G") were measured. The outer edge of the sample was coated by a thin layer of silicon oil to prevent evaporation of water during measurements.

Equilibrium Swelling Ratio

The equilibrium swelling ratio was detected by recording the change in wet weight during incubation in PBS at pH 7.4. The mass of the original wet hydrogels was recorded as W_0. The hydrogels were then incubated in PBS at 37°C. At different time points, the hydrogels were extracted from the PBS, and the quality was recorded as W_t. The swelling rate was calculated as $(W_t-W_0)/W_0 \times 100\%$. Repeat measurements of at least three independent samples were made to ensure reproducibility.

In vivo Degradation Analyses

For in vivo degradation studies, 0.5 mL hydrogels were surgically implanted under the skin of the back of rats. After the rats were sacrificed at the specified time points of 1, 4, 7, 14, 21, 28, 35, 42, 49 and 56 days, the remaining hydrogels were collected for photo-graphing and quality measurement. At the same time, the skin in contact with the hydrogel was subjected to hematoxylin-eosin (H&E) staining to observe whether the hydrogels caused an inflammatory response in vivo.

Vancomycin Release Study

Transferred the prepared 1mL the Van/Gel into a dialysis bag (MWCO 10000Da), sealed it securely, and then placed it into a centrifuge tube containing 5 mL PBS. The centrifuge tube was placed in an incubator shaker at a constant temperature and a speed of 120.0 r/min. Collected 200 μL of soaking solution on days 1, 4, 7, 14, 21, 28, 35, 42, 49, and

56, respectively. Subsequently, added 200 μL of fresh PBS and continued with agitation. The concentration of vancomycin in the soaking solution was measured by an ultraviolet spectrophotometer (Shimadzu Company, Japan) at a wavelength of 280nm.

$$A_X = \frac{C_x \times V + v \times \left(\sum_{t=1}^{x-1} C_t\right)}{C_0 \times V}$$

A_X represents the cumulative emission rate on the xth day; C_0 represents the concentration of vancomycin in the hydrogels on 0 day, and in this experiment, C_0 is set at 50 mg/mL; V represents the total volume of the soaking solution, and in this research, V is defined as 5 mL; Cx represents the concentration of vancomycin in the soaking solution on the xth day; v represents the total volume of soaking solution collected at each time point, and in this study, v is specified as 0.2 mL; x-1 represents the predetermined time point for the collection of soaking solution immediately before the xth day; C_t represents the concentration of vancomycin in the soaking solution on the tth day.

In vitro Experiment

Cell Proliferation and Cell Viability

To study the bio-compatibility of the Van/Gel, calcein-AM/PI staining and the CCK-8 assay were performed. MC3T3-E1 cells were seeded at 5×10^3 cells/mL on a control group (Con), a pure hydrogels group (Gel), and the Van/Gel in 24-well plates. For the CCK-8 assay, MC3T3-E1 cells were co-cultured with hydrogels for 1, 3, and 7 days. At each time point, the medium was replaced in each group, and 10% of the medium volume of CCK-8 reagent was added and incubated for 2 hours in the dark. Absorbance was subsequently monitored at a wavelength of 450 nm.

For calcein-AM/PI staining, after incubating at 37 °C for 1 day and 3 days, a working solution of calcein-AM/PI stain was prepared according to the manufacturer's instructions. After immersion for 15 minutes at 4 °C in the dark, the working solutions were re-moved, and the samples were washed twice with PBS to eliminate redundant staining. The stained cells were observed under a fluorescence microscope.

Hemolysis Assays

Hemolysis assays were performed according to the previous studies.[30] Red blood cells were isolated from fresh rabbit blood and diluted to 2% with 0.9% NaCl solution. Diluted red blood cells (1 mL) were mixed with 0.9% NaCl solution (1 mL) as the negative control and DI H_2O (1 mL) as the positive control. Then Gel and Van/Gel (100 μL) were mixed with diluted red blood cells (1 mL) to form the experimental samples. Three hours later, the absorbance of the supernatants at 541 nm was determined on a microplate reader.

Antibacterial Agar Experiment

Escherichia coli (E. coli) (ATCC25932) and methicillin-resistant *Staphylococcus aureus (MRSA)* (ATCC43300) were selected to detect the antibacterial properties of the Van/Gel. First, the cultured *E. coli* and *MRSA* were diluted to about 1×10^8 CFU/mL. The 0.8 mL bacterial suspension was evenly spread on an agar culture dish. Then the same volume (30 μL) of Gel and Van/Gel was placed on the agar plate. After incubation for 24 hours, the size of the inhibition of zone (ZOI) was observed.

Bacterial Vitality

In order to further quantify the antibacterial performance of the Van/Gel, a growth curve experiment of a co-culture of bacteria and hydrogels were carried out. First, the same volume (1 mL) of Gel and Van/Gel were formulated separately in bacterial culture tubes. Then, the suspension of *E. coli* and *MRSA* (1×10^8 CFU/mL, 3 mL) was uniformly inoculated into a bacterial culture tube. The group containing only bacterial suspension was the control group. All groups were cultured at 37 °C, 100.0 r/min. Samples (100 μL) were collected at 0, 4, 8, 12, 24, 36, and 48 hours after culture. The optical density of the bacterial suspension was read at 600 nm using a microplate reader. In order to observe the number of colonies after 24 hours of culture, the bacterial suspension was diluted and the diluent (100 μL) was evenly coated on the agar plate. The plate was placed in an environment of 37 °C and the colonies were photographed using a digital camera. The number of bacteria was analyzed using Image J software.

At the same time, in order to observe the vitality of bacteria, bacteria cultured for 24 hours were stained with bacterial live/death staining. The bacteria in each group were collected by centrifugation and washed three times with 0.85% sodium chloride solution to remove the excess medium. Then stained with live/dead bacterial staining kit according to the manufacturer's procedures, and the bacterial staining results were observed under a fluorescence microscope.

Animal Experiment

Development of an Infected Bone Defect Model

All procedures involving rats adhered to the "Guidelines for the Ethical Review of Laboratory Animal Welfare" provided by the Institutional Animal Care and Use Committee of Jilin University (Changchun, P. R. China, NO. KT202106016). A rat femoral infected bone defect model was established for the in vivo experiment. Thirty-three 6-week-old male Wistar rats were randomly divided into defect (3 rats) and infection (30 rats) groups. In the defect group, only the femur defect was treated. To establish an infected bone defect model, the rat was placed in an induction chamber and subjected to an induction dose of 4% isoflurane at a rate of 1.0 L/min until reflex loss occurred, followed by a maintenance dose of 2% isoflurane at a rate of 0.2 L/min. The surgical incision was made 1.5 cm below the right greater trochanter of femur, and the soft tissues were gently separated to expose the femur. A 2.5 mm diameter rotary head was used to rotate the femur, and a curved needle was used to remove part of the bone marrow. At the same time, 0.1 mL of 5% sodium morrhuate was injected into the bone marrow cavity. Then a gel sponge with the same size was placed into the bone marrow cavity and sealed with bone wax (Figure S1). The gel sponge was preincubated in a 1×10^7 CFU/mL suspension of *MRSA*. The wound was closed with an absorbable suture. No antibiotics were used postoperatively.

At 1, 2, 3, and 4 weeks after bacterial implantation, the wound condition of each rat was observed and wound healing was evaluated. Four weeks after bacterial implantation, three rats were sacrificed, and the femur was fully exposed and completely removed along the original surgical incision approach. The removed rat femur was fully ground and pulverized, placed in a beaker filled with PBS, shaken (1200 r/min) and rinsed for 5 minutes. Then, 100 μL solution was inoculated on an agar plate and cultured at 37 °C for 24 hours to observe whether bacteria could be cultured. At the same time, the cultured bacteria were subjected to Gram staining.

Implantation of the Van/Gel

Four weeks after the first surgery, debridement surgery was performed. The femur was re-exposed in the same surgical manner, and all nonviable soft tissues were completely excised. Then, the wound was washed with iodophor disinfectant and 0.85% NaCl solution. In the process of debridement, obvious infection can be observed. Finally, the syringes were used to inject 0.3 mL sterile the Gel and Van/Gel into the femoral defect of rats. The skin was then sutured. The Con group only underwent thorough debridement without injection of any material.

Assessment of Therapeutic Effect

Four and eight weeks after the second operation, three rats in each group were sacrificed. The femur was fully exposed and completely removed along the original surgical incision approach. The femur was fully ground up and pulverized, placed in a beaker filled with PBS, shaken (1200 r/min) and rinsed for 5 minutes. Then, bacterial culture was performed and the number of bacterial colonies was observed after 24 hours of culture at 37 °C.

Imaging Analysis

In order to evaluate bone regeneration, the intact femur was collected 8 weeks after implantation, and the samples were examined by micro-computed tomography (micro-CT). The scanning parameters were as follows: 90 kV voltage, 114 mA current, and a pixel size of 18 μm. The bone defect area was selected as the region of interest (ROI) for 3D reconstruction and parameter analysis. To further evaluate the quality of bone in-growth, the BV/TV, Tb.N, Tb.Sp and trabecular thickness (Tb.Th) of the ROI were analyzed and compared among the groups.

Biomechanical Analysis

The samples were mounted in potting blocks filled with Wood's metal and compressive stiffness was assessed with an MRTP-0.2NM force transducer (Interface) interfaced with an ELF 3200 (Bose) mechanical testing system running

WinTest7. In addition, we evaluated the torque-to-fault angle. A continuous ramp function of 3°/s was applied and the highest recorded torsion angle was recorded.

Histological Analysis

All specimens were fixed in 4% paraformaldehyde solution for 1 week and decalcified with 17% EDTA solution for 5 weeks. Sagittal slices with a thickness of 3.0 μm were made and stained with H&E and Masson's trichrome to observe local tissue morphology and bone regeneration and integration. In addition, to evaluate infection around the bone defect, Giemsa staining was performed to check for bacterial contamination.

Statistical Analysis

The data from three independent experiments are presented as the mean ± standard deviation (SD) and used for statistical analyses. Student's *t*-test or one-way analysis of variance was performed to determine the variation between groups using SPSS 26.0 software (SPSS Inc., Chicago, USA). Statistical significance was set at $p < 0.05$ ($*p < 0.05$, $**p < 0.01$, $***p < 0.001$).

Results and Discussion

Characterization of the Van/Gel

Following the aldehyde titration method reported previously, the degree of oxidation of the ODEX was determined to be 30%.[31] The sustained-release system carrier was prepared by crosslinking the four-arm PEG-NH_2 with ODEX (Figure 1A). The PEG/ODEX hydrogels exhibited good gelling properties at room temperature (Figure 1C). Under ambient temperature conditions, the mixture of two solutions can form the PEG/ODEX hydrogels within 1 minute. Consequently, we can prepare the Van/Gel on the surgical table based on the injury site, which is crucial for hydrogel storage and reducing surgical exposure time.

The infrared spectrum of hydrogels is shown in Figure 1B. The broad peak at 3341 cm^{-1} corresponds to the stretching vibration of the hydroxyl O-H groups in PEG and ODEX. The vibration peak at 1637 cm^{-1} comes from the stretching vibration of the C=O double bond of the aldehyde group on ODEX and the C=N bond of the Schiff's base reaction.

The rheological properties of the hydrogels were further characterized. As shown in Figure 1D, the G' was higher than the corresponding G", which means that hydrogels can return to their original state and maintain their shape after being deformed. This is crucial for applications of hydrogels in tissue engineering and drug delivery as it can help to provide support and stability.[32]

To explore the morphological nature of the cross-linking structure, the hydrogels were imaged using SEM to reveal a homogeneous and highly porous structure that formed channels, with pore size ranging from 60 to 100 μm (Figure 1E). This porous structure guaranteed vancomycin loading and controlled release. In addition, these channels could benefit oxygen and nutrient transportation, thereby improving cell survival and communication, which has important value for biological applications.[33,34]

EDS surface scanning results showed that the main components of the hydrogels were Na, C, O, and Cl, and all these elements were uniformly distributed (Figure 1F). Na and Cl were assumed to be components of PBS. The EDS point scanning results showed that the two most common elements of the hydrogels were O and C, in that order (Figure 2A).

The swelling characteristics of the hydrogels under physiological conditions were investigated. The hydrogels could reach swelling equilibrium in about 24 hours, and the maximum swelling rate was about 32.5% ± 2.8% (Figure 2B). Furthermore, the hydrogels maintained their original shape during swelling. This physical and chemical stability is ideal for implantation.[35] Such a swelling rate contributes to maintaining the stability of hydrogels to a certain extent, preventing excessive swelling or disintegration during usage. Additionally, a moderate swelling rate facilitates precise control over drug release, ensuring the stability of the release rate and thereby contributing to the maintenance of therapeutic effectiveness.[36]

Amino groups and aldehyde groups commonly form functional chemical bonds in hydrogel materials.[37] Amino groups can undergo Schiff base reactions with aldehyde groups, forming crosslinking structures and achieving stabilization of the hydrogels. This chemical bond is advantageous for controlled synthesis and customized design of

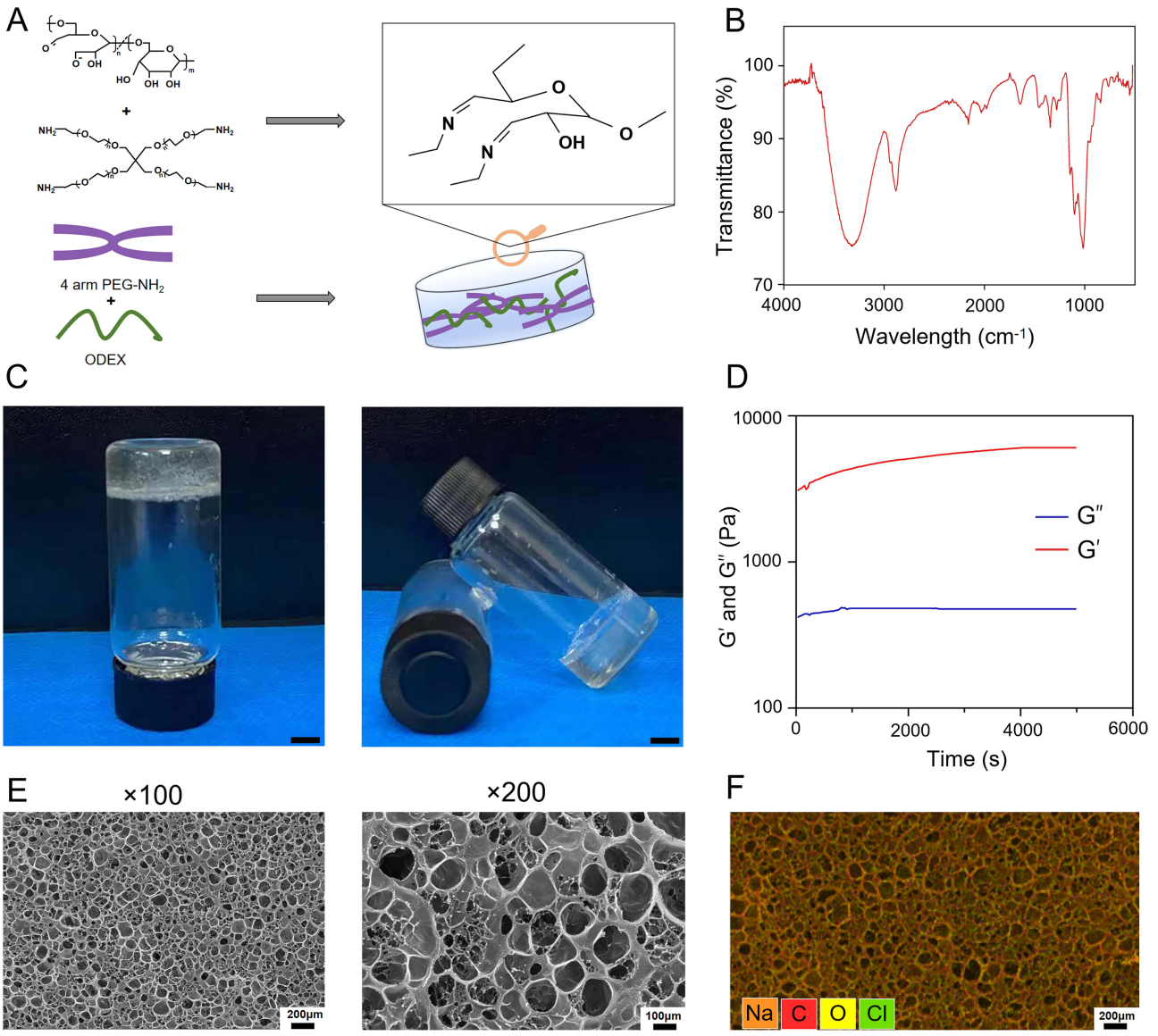

Figure 1 Synthesis and characterization of PEG/ODEX hydrogels. (**A**) Schematic diagram of hydrogel synthesis; (**B**) infrared spectrum of hydrogels; (**C**) external appearance image of the hydrogels; (**D**) rheological properties of the hydrogels; (**E**) representative scanning electron microscopy image of the hydrogels; (**F**) EDS surface scanning.

hydrogels.[38,39] Although the hydrogel we designed cannot be injected, it can be gelled in situ at the defect site. Therefore, we can still accurately place the hydrogel inside the bone marrow cavity.

The time course of degradation of PEG/ODEX hydrogels in rats is shown in the Figure 2C. In the preliminary experiments, we assessed the degradation rate of the hydrogels in vivo by gauging its size through tactile examination beneath the rat's skin. We observed a relatively slow degradation rate, and it was only after 56 days that the hydrogels became non-palpable. Consequently, we opted for longer intervals to monitor the degradation progress of the hydrogels. The hydrogels had strong water absorption and swelling capacity, and the weight of the implant increased to 0.87 ± 0.09 g on the third day. With the passage of time, the weight of residual hydrogels in rats gradually decreased. The hydrogels were almost completely degraded after 56 days of implantation (Figure S2). This process of degradation was relatively slow and uniform, which would facilitate sustained drug release. Previous studies indicated that individual imine bonds were unstable in aqueous environments.[40] However, when multiple imine covalent bonds are interconnected within the matrix network constituting the hydrogel, their stability is significantly enhanced.[41] The bone repair process imposes requirements on the degradation time of locally implanted

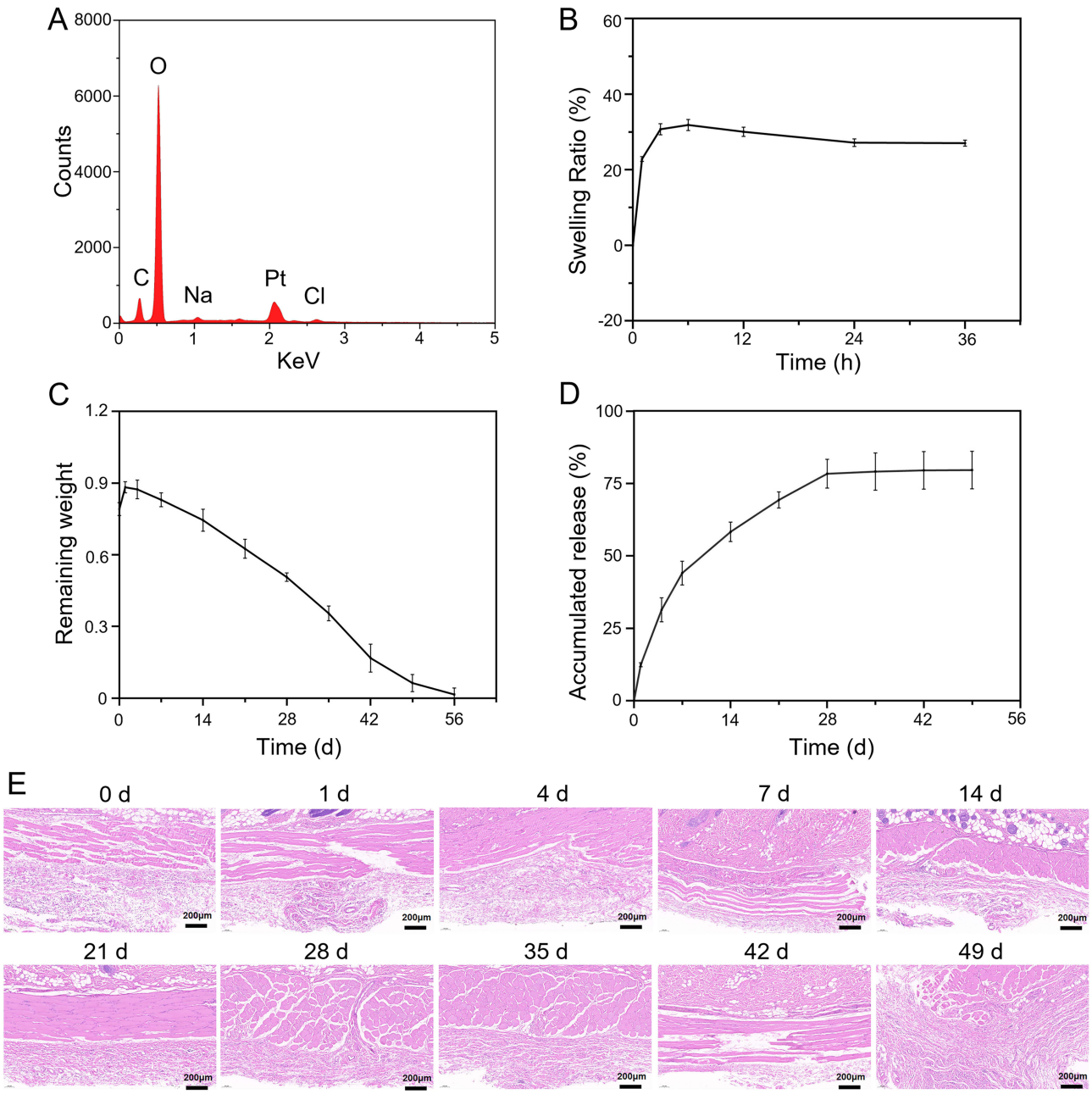

Figure 2 Characterization of PEG/ODEX hydrogels. (**A**) EDS point scanning; (**B**) swelling equilibrium of hydrogels; (**C**) degradation behaviour of hydrogels in vivo; (**D**) release profile of the Van/Gel; (**E**) hematoxylin-eosin staining of rat skin. All values are expressed as mean ± SD, n = 3.

materials. Prolonged occupation of the implant can hinder the growth of new bone tissue, leading to delayed fracture healing.[42] In the case of infection, bone repair may be delayed; hence, when treating infected bone defects, a slower degradation rate of the implant may be preferable.

For evaluation of inflammation, skin was stained with H&E. As shown in Figure 2E, neutrophil granulocytes aggregated around skin tissue during the first week at the incision used for hydrogel implantation. Inflammation gradually diminished with time after implantation, which demonstrated that the PEG/ODEX hydrogels possessed good biocompatibility in vivo.

Sustained Drug Release

The release profile of vancomycin is shown in Figure 2D. We studied drug-releasing kinetics over a 56-day period consistent with the time course of degradation and demonstrated a relatively sustained release profile. The total release percentage of vancomycin on the first and the third days was 10.4% ± 0.7% and 31.3% ± 3.8%, respectively, which represented slightly rapid initial release. Over the next 14 days, drug release increased to 58.3% ± 3.8%, illustrating satisfactory sustained release. By the 35th day, the drug released from the Van/Gel was 78.4% ± 3.2%, after which little drug was released from the Van/Gel.

The vancomycin embedded in the PEG/ODEX hydrogels matrix was primarily released into the surrounding environment through two mechanisms: free diffusion of the drug and release upon degradation of the material.[43,44] Analyzing the degradation curve of the PEG/ODEX hydrogels in conjunction with the drug release curve revealed that during the initial 7 days, the degradation rate of the PEG/ODEX hydrogels was relatively slow, and the release of vancomycin was primarily governed by free diffusion. During this period, vancomycin located in the surface layer was released more easily into the surrounding environment at a relatively faster rate. Furthermore, as indicated by the swelling experiments and in vivo degradation results, the PEG/ODEX hydrogels had strong water absorption and swelling capacity, which allowed vancomycin to easily diffuse out of the gel. The early rapid release phase allowed the drug to quickly reach an effective concentration in a short time, which facilitated the antibacterial effect of the drug-loaded hydrogels and did not affect subsequent sustained release of the drug. After the 7th day, there was a noticeable acceleration in the degradation rate of the PEG/ODEX hydrogels, and the release of vancomycin was predominantly governed by the degradation of the material. This allowed the vancomycin located within the hydrogels to be released into the surrounding environment. As the material degraded, the content of vancomycin gradually decreased, leading to a reduction in both the amount and rate of drug release.

In this study, we engineered the Van/Gel with a concentration of 50 mg/mL vancomycin, and applied 1 mL of the hydrogels 1cm^3 of the environment. Based on the drug release kinetics, the Van/Gel exhibited an average release of approximately 5.2 mg of vancomycin on the first day (10.4%). Subsequently, the average daily release rate was approximately 2.5%. This maintained the concentration of vancomycin within the microenvironment at around 1.2 mg/mL. This concentration still significantly exceeds the minimum inhibitory concentration of vancomycin, making it crucial for the eradication of infections.[45] When infection exists, normal bone repair will not exist.[46] Therefore, we chose a higher concentration of vancomycin as much as possible. According to previous studies, 50 mg/mL vancomycin could restore the infected site to a sterile state as soon as possible.[47] It was reported that a concentration of vancomycin over 5.0 mg/mL leads to toxicity in corneal endothelial cells.[48] The vancomycin released by the Van/Gel reached a concentration of 5.2 mg/mL only on the first day, entering a subsequent slow-release phase where the local vancomycin concentration significantly decreased. In addition, during subsequent cell proliferation experiments, we did not observe any toxicity in cell performance from the Van/Gel. Therefore, to promptly eliminate the infection, we opted for this concentration of vancomycin.

Non-Toxic Effects on Cell Proliferation and Viability

The CCK-8 assay was performed to quantitatively evaluate the effect of the Van/Gel on cell proliferation. In Figure 3B, cells in each group exhibited favorable growth within 7 days. No significant differences were noted in the number of cells among the various groups at days 1, 3, and 7, which indicated that the Van/Gel had a negligible effect on cell proliferation.

The effect of the Van/Gel on cell viability was assessed via calcein-AM/PI staining. As shown in Figure 3A, living cells stained with calcein-AM emitted green fluorescence, while dead cells stained with PI emitted red fluorescence. The staining of living MC3T3-E1 in each group increased from days 1 to 3. No significant differences were noted in the number of living cells among the Con, Gel and Van/Gel groups.

In order to further verify the biocompatibility of the Van/Gel, a hemolysis test was performed. As shown in Figure 3C, Gel and Van/Gel did not cause obvious hemolysis. The hemolysis rate in all groups was < 5%, which indicated that the hydrogels were compatible with the cells.

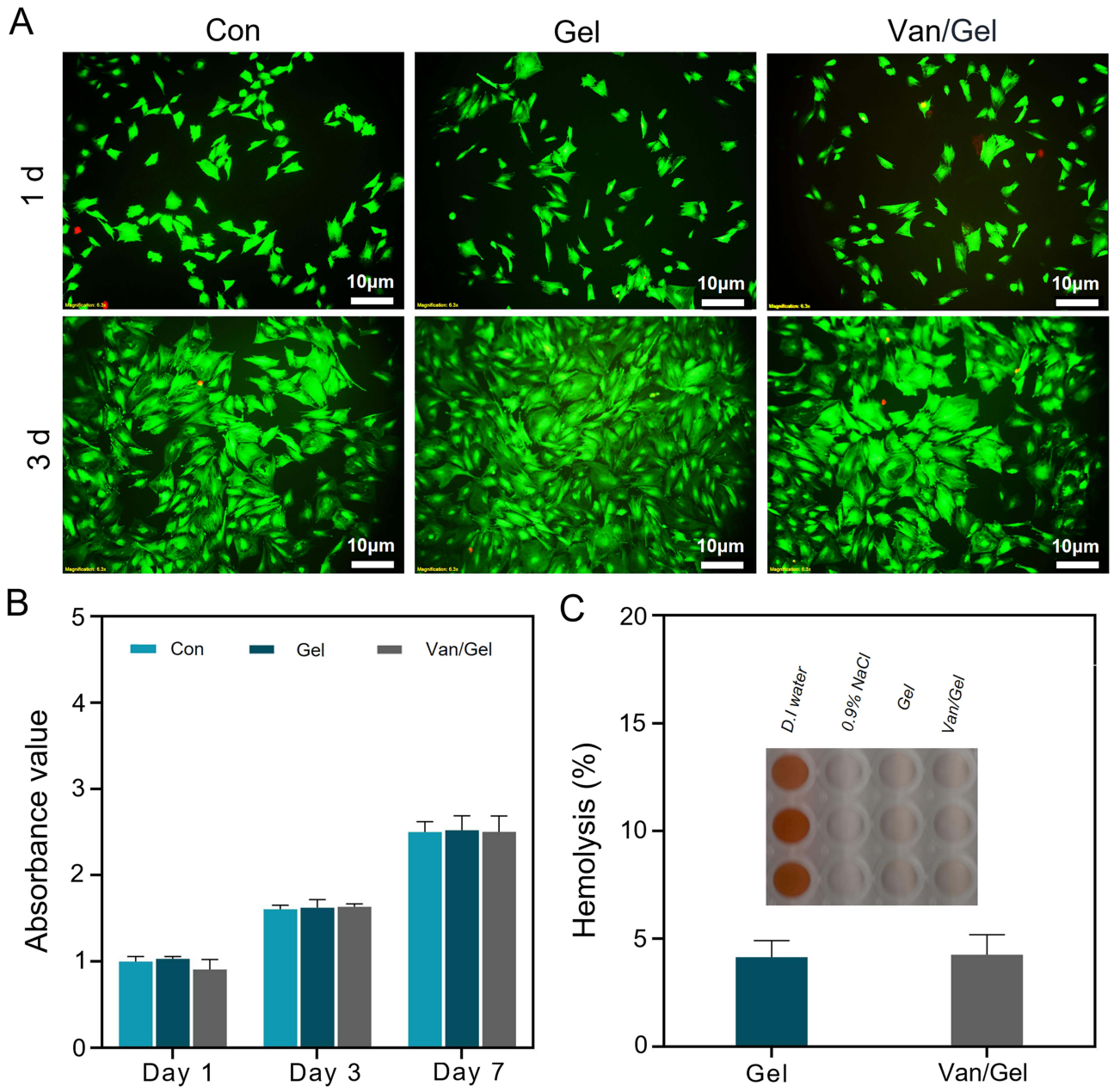

Figure 3 Biocompatibility of the Van/Gel in vitro. (**A**) Representative image of calcein-AM/PI staining; (**B**) CCK-8 analysis of MC3T3-E1 cells number; (**C**) Hemolysis of the Gel and Van/Gel. All values are expressed as mean ± SD, n = 3.

Excellent cell compatibility is the basis for in vivo applications. Cell proliferation and cell activity are important indicators for evaluating whether a sustained-release system has favorable biological characteristics.[49,50] The above results confirmed that the Van/Gel had no significant effect on cell proliferation and cell activity. The system thus meets the criteria for use in vivo.

Antibacterial Properties of the Van/Gel

After confirming the cytocompatibility of the Van/Gel, this study also evaluated the antibacterial effect of the vancomycin release system. *E. coli* and *MRSA* are common species causing osteomyelitis.[51,52] To verify the in vitro antibacterial effect of the vancomycin release system, an antibacterial agar experiment was first performed. As shown in Figure 4A, an obvious ZOI was observed in the Van/Gel group when compared with the Gel group. The diameter of

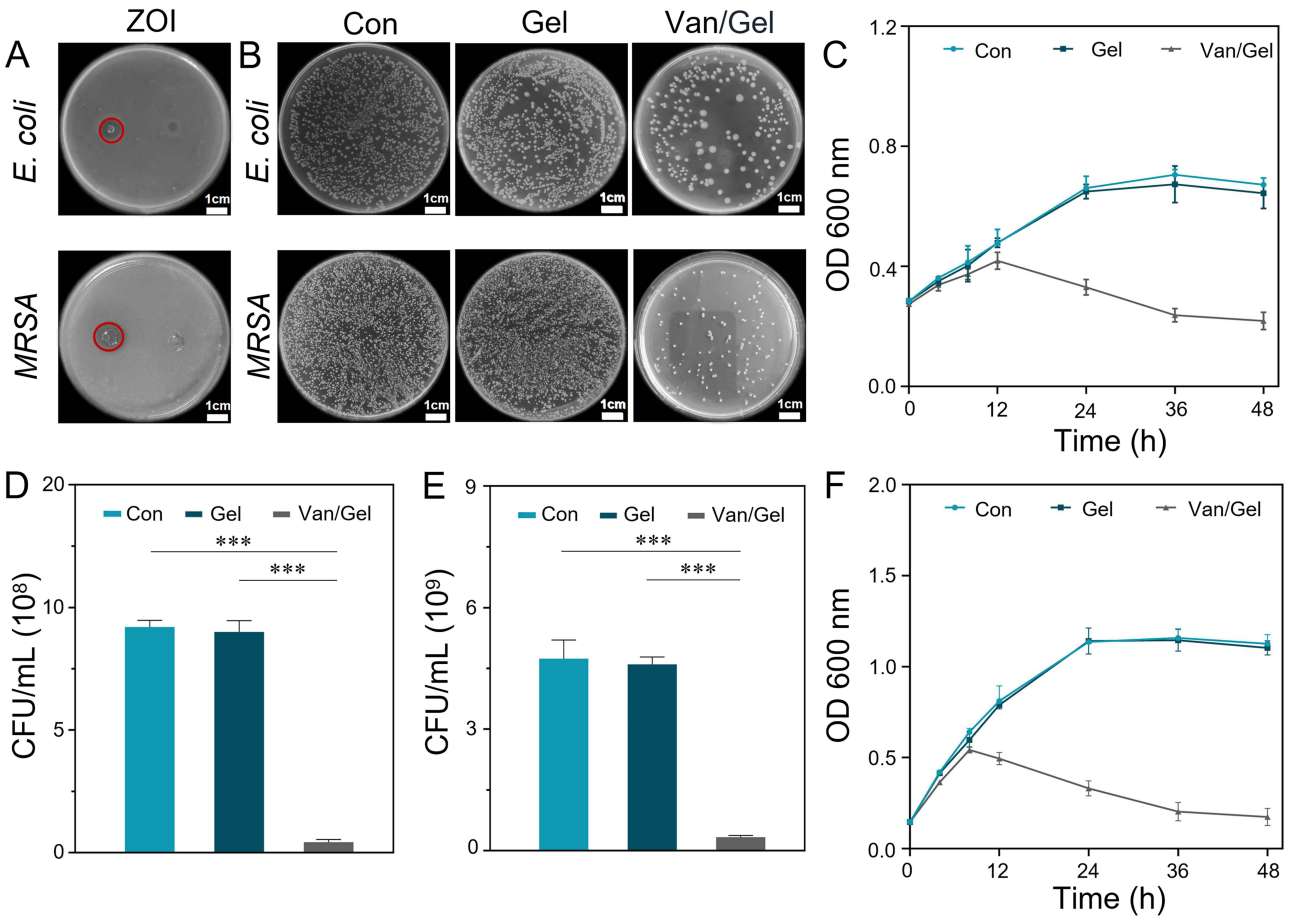

Figure 4 Antibacterial ability of the Van/Gel in vitro. (**A**) The ZOI of the Gel and Van/Gel groups (The red circle represents ZOI.); (**B**) Bacterial coating experiment after 24 hours co-incubation; (**C**) The growth curve of *E. coli* within 48h; and (**D** and **E**) Quantitative analysis of bacterial coating experiment; (**F**) The growth curve of *MRSA* within 48h. (***$p < 0.001$). All values are expressed as mean ± SD, n = 3.

the ZOI for *MRSA* group was approximately 1.37 cm, while for *E. coli* group, it was approximately 1.25 cm. However, in the Gel group, the appearance of ZOI was almost non-existent. This result initially confirmed the ability of the complex system to eliminate infection.

As shown in Figure 4B, after 24 hours solid culture of bacteria in each group, we found that both the Con and Gel groups were overgrown with bacteria, while the number of colonies in the Van/Gel group was significantly less. For image analysis, the concentration of *E. coli* was approximately $9.23 \pm 0.21 \times 10^8$ CFU/mL in the Con group and about $9.10 \pm 0.12 \times 10^8$ CFU/mL in the Gel group, both of which were significantly greater than in the Van/Gel group ($0.43 \pm 0.11 \times 10^8$ CFU/mL) (Figure 4D). The concentration of *MRSA* was approximately $4.73 \pm 0.47 \times 10^9$ CFU/mL in the Con group and about $4.60 \pm 0.21 \times 10^9$ CFU/mL in the Gel group, which were significantly greater than in the Van/Gel group (Figure 4E). These results demonstrated the antibacterial effect of the Van/Gel.

We evaluated the in vitro antibacterial efficacy of the vancomycin release system by measuring absorbance to assess bacterial proliferation. As shown in Figure 4C–F, the Van/Gel had no obvious antibacterial effect for the first 8 hours. As the release of vancomycin increased, the absorbance decreased significantly after 12 hours, indicating that the Van/Gel was beginning to perform well. The Con and Gel groups of bacteria grew and multiplied normally. During the initial 8 hours, bacteria might have undergone an exponential growth phase, while the release rate of the Van/Gel medication was insufficient to reach the MIC required for bacterial suppression, thus failing to effectively inhibit bacterial growth.[43] As time progressed, the growth rate of bacteria gradually slowed down, eventually reaching a plateau phase. At that point,

the concentration of vancomycin released through free diffusion also gradually increased, effectively eliminating bacteria.

Figure 5A–C shows more intuitively the viability of each group of bacteria. After 24 hours of co-culture, almost no dead bacteria (red) were observed in the Con and Gel groups, while most of the bacteria in the Van/Gel group had died. For image analysis, it was found that the mortality rate of *E. coli* in the Van/Gel group was 65.47% ± 2.9%, and the mortality rate of *MRSA* bacteria was 83.77% ± 1.9% (Figure 5B–D). The initial release of vancomycin from the antibacterial hydrogels was sufficient to inactivate all *MRSA* in the system, so they could not continue to proliferate. However, the inhibitory effect of antibacterial hydrogel on *E. coli* was somewhat different.

Considering that vancomycin belongs to the glycopeptide class of antibiotics, its primary mechanism of action involves blocking the synthesis of peptidoglycan, a polymer that constitutes bacterial cell walls, leading to cell wall damage and bacterial death.[53] The relatively thin cell wall of *MRSA* makes it easier for vancomycin to penetrate and exert its effects. In contrast, *E.coli* has a cell wall composed of components such as lipopolysaccharides, making it structurally

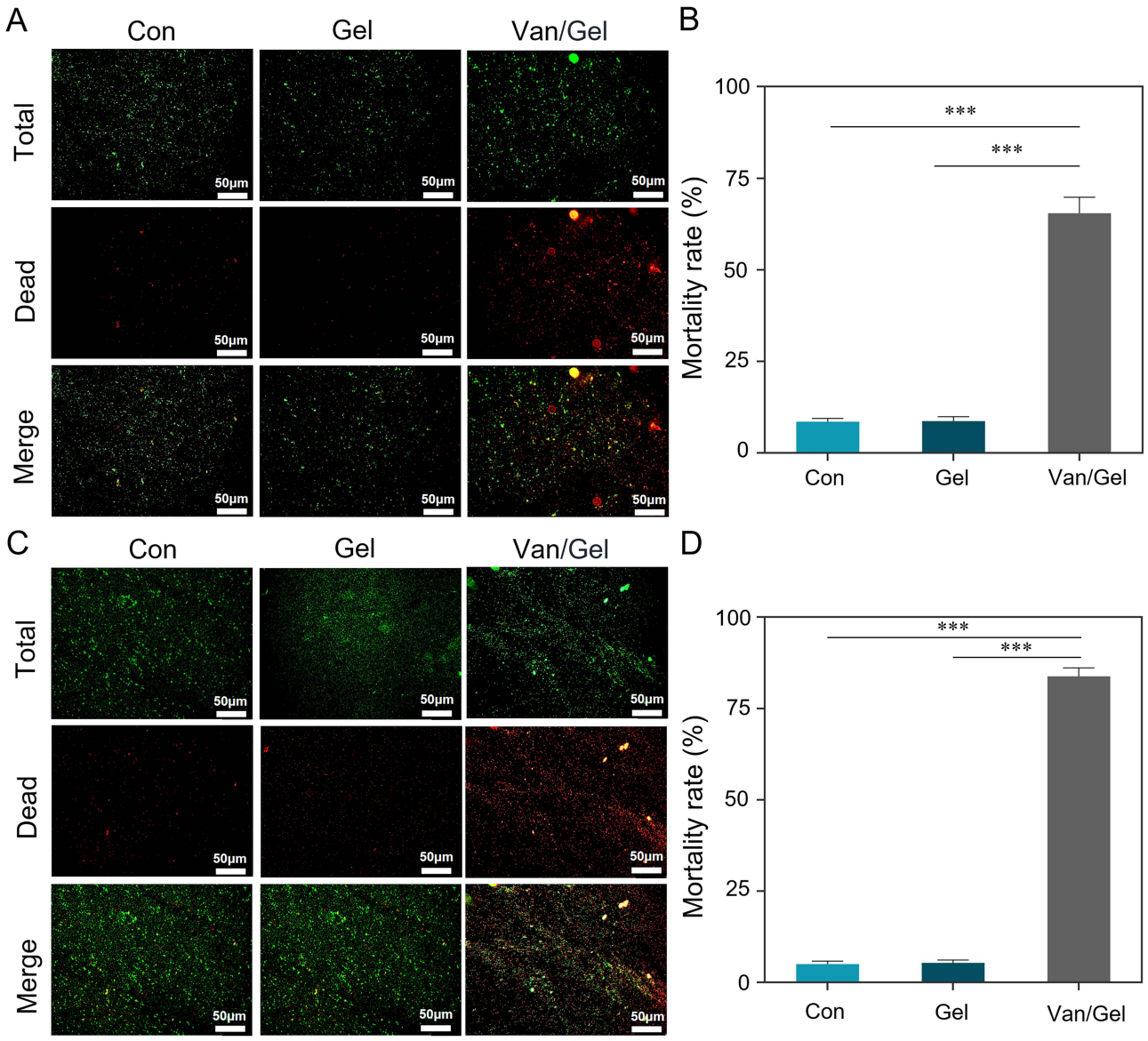

Figure 5 The viability of each group of bacteria. (**A**) Representative image of *E. coli* activity and (**B**) quantitative analysis; (**C**) Representative image of *MRSA* activity and (**D**) quantitative analysis. (***$p < 0.001$). All values are expressed as mean ± SD, n = 3.

more complex and potentially more resistant to vancomycin penetration.[54] Therefore, vancomycin's antibacterial effect may be more pronounced against *MRSA*.

The above results indicate that Van/Gel can remove *E. coli* and *MRSA* by releasing an effective concentration of vancomycin. Compared with the most widely used PMMA bone cement in clinical practice, the hydrogels we applied not only had a favourable degradation curve, but also excellent antibacterial properties.[55,56] Thus, it can be regarded as a reasonable substitute for PMMA bone cement.

Animal Experiment

After 1 week of bacterial implantation, we observed inflammatory reactions near the wounds of the rats. Four weeks later, pyorrhea occurred near the wounds, and a sinus tract appeared in some of them (Figure S3). At this time, the rat femur specimens placed in bacterial culture, which yielded positive results (Figure S4A). Bacterial Gram staining experiments showed that the infection was caused by Gram-positive bacteria (Figure S4B). The above results indicated that the rat model of the infected bone defect was successfully established.

Our formulation allows for in situ polymerization of the hydrogel that adheres to the exposed tissue and fracture surfaces, which is important for treating complex infective fractures. To test for an antibacterial effect in vivo, the number of bacteria in each group was determined by the plate coating method. As shown in Figure 6A and B, the number of colonies in the Van/Gel group was significantly lower than in the Con and Gel groups, both 4 and 8 weeks after material implantation. It is worth noting that at 8 weeks, almost no bacteria were cultured in the Van/Gel group. This indicates that Van/Gel can effectively control bacterial growth at the site of infection.

After 8 weeks of implantation, rat femur specimens were collected for micro-CT scanning. The 3D images revealed the bone defects in each group. There was no obvious sign of bone defect healing in the Con and Gel groups. The bone defects in the Van/Gel group were largely healed and bone regeneration was clearly present. Two-dimensional images also confirmed this trend (Figure 6C). In order to further evaluate bone repair, we calculated the relevant parameters of the femoral ROI by 3D reconstruction of the scanned image. The 3D image analysis of the Van/Gel group showed that the BV/TV was 1.39-fold higher ($p < 0.001$), the Tb.N was 1.31-fold higher ($p < 0.05$), and the Tb.Sp was 0.58-fold higher than those of the Con group ($p < 0.01$). The results of the Gel group were similar to those of the Con group (Figure 6D–F). The micro-CT results indicated that bone defects in the infectious microenvironment did not regenerate effectively in the Con and Gel groups, while the Van/Gel could significantly improve bone formation.

As shown in Figure 6G, at 8 weeks, the compressive stiffness of the Van/Gel group had increased by 2.99-fold ($p < 0.001$) compared with the Con group, and by 2.65-fold compared with the Gel group ($p < 0.001$). The highest torsion angle of the Van/Gel group had also increased by 2.09-fold ($p < 0.01$) compared with the Con group and increased by 2.93-fold compared with the Gel group ($p < 0.01$) (Figure 6H). Therefore, in the rat model of fracture infection, the Van/Gel cleared infections and supported fracture repair leading to recovery of bone mechanical properties.

H&E and Masson staining of the decalcified femur specimens showed histological morphology of the femur in detail. The results of H&E staining showed that there was still inflammation and disordered arrangement of tissue fibres in the Con and Gel groups at 8 weeks after the operation. Compared with the Con and Gel groups, inflammation was better controlled in the Van/Gel group (Figure 7A). Masson staining showed formation of new bone in the Van/Gel group, and there were a large number of osteoblasts around the bone tissue (Figure 7B). In the Giemsa staining image of the Con and Gel groups, a large number of bacteria were observed (indicated by red arrows), showing that the infection was not under control. However, few bacteria were observed in the Van/Gel group (Figure 7C). Thus, sustained release of vancomycin can effectively remove bacteria at the site of infection, transforming the bone defect site into a sterile microenvironment for osteogenesis.[57]

Infection negatively affects bone tissue in patients, and a persistent inflammatory environment can inhibit bone tissue regeneration.[58] Therefore, we established a rat model of an infected bone defect to verify the therapeutic effect of the Van/Gel in vivo. Clearing infection is the primary requirement for bone repair in

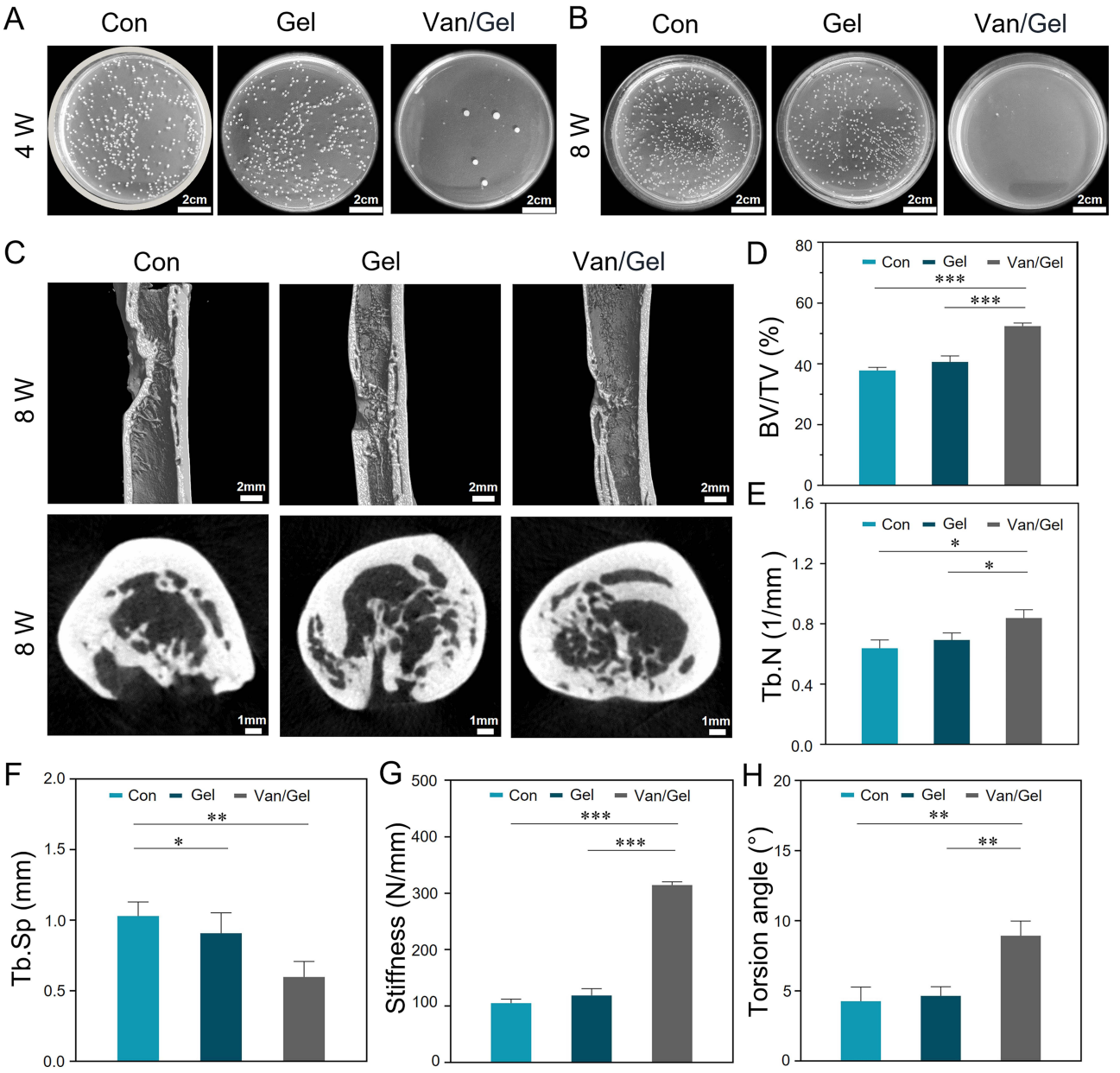

Figure 6 Assessment of therapeutic effect in vivo. (**A** and **B**) Bacterial coating experiment after hydrogel implantation for 4 weeks and 8 weeks; (**C**) Representative 3D images and cross-sectional images of bone defects and (**D**) volume fraction (BV/TV); (**E**) trabecular number (Tb.N); (**F**) trabecular separation (Tb.Sp); (**G**) compressive stiffness for each group, and (**H**) the highest torsion angle for each group. (*$p < 0.05$, **$p < 0.01$, ***$p < 0.001$). All values are expressed as mean ± SD, n = 3.

infected bone defects. Bacterial exotoxins and enzymes can directly impair osteocytes and surrounding tissues, leading to bone marrow necrosis and destruction of bone tissue.[59,60] If the lesion continuously experiences an infected microenvironment, local osteogenic ability is almost non-existent.[61] In this study, the composite material was found to have no impact on cell adhesion and proliferation. Moreover, it showed no toxic effects in vivo and effectively eradicated infections through sustained local antibiotic release, thereby enhancing the local micro-environment of bone defects. Additionally, the Van/Gel was biodegradable and eliminated the need for secondary surgery. In summary, the Van/Gel demonstrated the potential to treat infected bone defects.

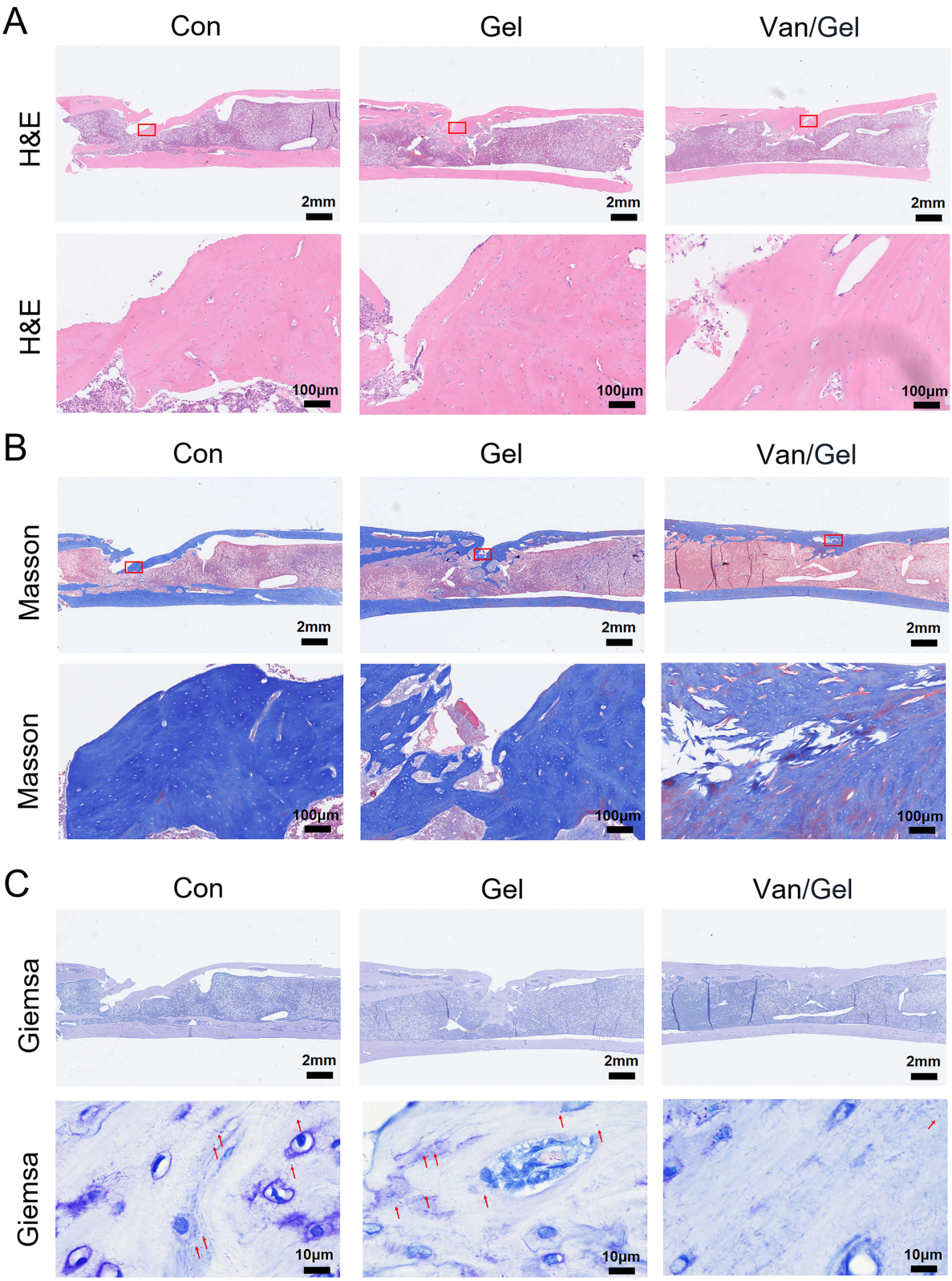

Figure 7 Histological staining of femoral defects in rats. (**A**) H&E staining of rat femur, with the red borders in the upper row of images indicating the location of the magnified images in the lower row; (**B**) Masson staining of rat femur, with the red borders as for (**A**); (**C**) Giemsa staining of rat femur, red arrows indicate bacteria.

Conclusion

In this work, PEG/ODEX hydrogels were prepared by Schiff base reaction, and vancomycin was loaded into them to construct a drug delivery system with controllable release and biodegradability; and then comprehensively evaluated from the material, cytology, bacteriology, and zoology perspective. The system had suitable physical and chemical properties, with vancomycin continuously releasing for 35 days, maintaining a concentration of approximately 1.2 mg/mL within the surrounding environment of bone defects. In vitro experiments, the drug delivery system exhibited good compatibility and satisfactory antibacterial effects against *E. coli* and *MRSA*. In the rat model of an infected bone defect, the Van/Gel provided excellent therapeutic efficacy, with bone repair clearly occurring after the infection was effectively controlled.

This study revealed the therapeutic effect of the Van/Gel on infected bone defect and expanded the research and application of bone tissue engineering for conditions associated with bone infections. The Van/Gel provides new materials and methodologies for treating infected bone defect, bearing crucial scientific significance and holding substantial value for clinical applications.

Funding

This work was financially supported by the Wu Jieping Medical Foundation (320.6750.2021–11–6). The project of Jilin Provincial Science and Technology Department (20230402009GH); Industrial Technology Research and Development Project of Jilin Provincial Development and Reform Commission(2023C040-3). The 13th Five-Year Plan of Science and Technology Research of Jilin Provincial Education Department (JJKH20180108KJ).

Disclosure

The authors report no conflicts of interest in this work.

References

1. Zhang Y, Zhou J, Wu J-L, et al. Intrinsic antibacterial and osteoinductive sterosomes promote infected bone healing. article. *J Control Release*. 2023;354:713–725. doi:10.1016/j.jconrel.2023.01.058
2. Banerjee J, Seetharaman S, Wrice NL, Christy RJ, Natesan S, Song J. Delivery of silver sulfadiazine and adipose derived stem cells using fibrin hydrogel improves infected burn wound regeneration article. *PLoS One*. 2019;14(6):e0217965. doi:10.1371/journal.pone.0217965
3. Johnson CT, Wroe JA, Agarwal R, et al. Hydrogel delivery of lysostaphin eliminates orthopedic implant infection by staphylococcus aureus and supports fracture healing. article. *Proc Natl Acad Sci USA*. 2018;115(22):E4960–E4969. doi:10.1073/pnas.1801013115
4. Wroe JA, Johnson CT, Garcia AJ. Bacteriophage delivering hydrogels reduce biofilm formation in vitro and infection in vivo article. *J Biomed Mater Res Part A*. 2020;108(1):39–49. doi:10.1002/jbm.a.36790
5. Cahill SV, Kwon H-K, Back J, et al. Locally delivered adjuvant biofilm-penetrating antibiotics rescue impaired endochondral fracture healing caused by mrsa infection article. *J Orthop Res*. 2021;39(2):402–414. doi:10.1002/jor.24965
6. Pu Y, Lin X, Zhi Q, Qiao S, Yu C. Microporous implants modified by bifunctional hydrogel with antibacterial and osteogenic properties promote bone integration in infected bone defects. article. *J Functional Biomaterials*. 2023;14(4):226. doi:10.3390/jfb14040226
7. Nie R, Sun Y, Lv H, et al. 3D printing of MXene composite hydrogel scaffolds for photothermal antibacterial activity and bone regeneration in infected bone defect models. article. *Nanoscale*. 2022;14(22):8112–8129. doi:10.1039/d2nr02176e
8. Peng K-T, Chen C-F, Chu I-M, et al. Treatment of osteomyelitis with teicoplanin-encapsulated biodegradable thermosensitive hydrogel nanoparticles. article. *Biomaterials*. 2010;31(19):5227–5236. doi:10.1016/j.biomaterials.2010.03.027
9. von Hertzberg-Boelch SP, Luedemann M, Rudert M, Steinert AF. PMMA bone cement: antibiotic elution and mechanical properties in the context of clinical use. review. *Biomedicines*. 2022;10(8):1830. doi:10.3390/biomedicines10081830
10. Hasan R, Wohlers A, Shreffler J, et al. An antibiotic-releasing bone void filling (ABVF) putty for the treatment of osteomyelitis. *Materials*. 2020;13(22):5080. doi:10.3390/ma13225080
11. Cui Y, Liu H, Tian Y, et al. Dual-functional composite scaffolds for inhibiting infection and promoting bone regeneration. *Mater Today Bio*. 2022;16:100409. doi:10.1016/j.mtbio.2022.100409
12. Liu X, Camilleri ET, Li L, et al. Injectable catalyst-free ”click” organic-inorganic nanohybrid (click-ON) cement for minimally invasive in vivo bone repair. *Biomaterials*. 2021:276121014. doi:10.1016/j.biomaterials.2021.121014
13. Li D, Huang Y, Shen H, Ma Y. Controlled antibiotic-loaded, drug-eluting implants for osteomyelitis. *Abstr Pap Am Chem Soc*. 2019;257 257.
14. Ullah I, Hussain Z, Ullah S, et al. An osteogenic, antibacterial, and anti-inflammatory nanocomposite hydrogel platform to accelerate bone reconstruction. article. *J Mat Chem B*. 2023;11(25):5830–5845. doi:10.1039/d3tb00641g
15. Pellegrini A, Legnani C. High rate of infection eradication following cementless one-stage revision hip arthroplasty with an antibacterial hydrogel coating. *Int J of Artificial Organs*. 2021;0391398821995507. doi:10.1177/0391398821995507
16. Chehreghanianzabi Y, Auner G, Shi T, et al. Impacts of compacting methods on the delivery of erythromycin and vancomycin from calcium polyphosphate hydrogel matrices. *J of Biomed Mater Res Part B-Applied Biomater*. 2022;110:412–421. doi:10.1002/jbm.b.34917

17. Navare KJ, Colombani T, Rezaeeyazdi M, et al. Needle-injectable microcomposite cryogel scaffolds with antimicrobial properties. *Sci Rep*. 2020;10(1):18370. doi:10.1038/s41598-020-75196-1
18. Makvandi P, Ashrafizadeh M, Ghomi M, et al. Injectable hyaluronic acid-based antibacterial hydrogel adorned with biogenically synthesized AgNPs-decorated multi-walled carbon nanotubes. *Progress Biomater*. 2021;10(1):77–89. doi:10.1007/s40204-021-00155-6
19. Liu S-M, Chen W-C, C-L K, et al. In vitro evaluation of calcium phosphate bone cement composite hydrogel beads of cross-linked gelatin-alginate with gentamicin-impregnated porous scaffold. *Pharmaceuticals*. 2021;14(10). doi:10.3390/ph14101000
20. Wang Z, Ye Q, Yu S, Akhavan B. Poly ethylene glycol (PEG)-based hydrogels for drug delivery in cancer therapy: a comprehensive review. *Review Adv Healthc Mater*. 2023;12(18).2370102
21. Chauhan N, Gupta P, Arora L, Pal D, Singh Y. Dexamethasone-loaded, injectable pullulan-poly(ethylene glycol) hydrogels for bone tissue regeneration in chronic inflammatory conditions. *Mater Sci Eng C-Mater Biol Appl*. 2021;130112463. doi:10.1016/j.msec.2021.112463
22. Mao X, Cheng R, Zhang H, et al. Self-healing and injectable hydrogel for matching skin flap regeneration. *Adv Sci*. 2019;6(3):1801555. doi:10.1002/advs.201801555
23. Censi R, Casadidio C, Dubbini A, et al. Thermosensitive hybrid hydrogels for the controlled release of bioactive vancomycin in the treatment of orthopaedic implant infections. *Eur J Pharm Biopharm*. 2019;142:322–333. doi:10.1016/j.ejpb.2019.07.006
24. Machado A, Pereira I, Silva V, et al. Injectable hydrogel as a carrier of vancomycin and a cathelicidin-derived peptide for osteomyelitis treatment. article. *J Biomed Mater Res Part A*. 2022;110(11):1786–1800. doi:10.1002/jbm.a.37432
25. Xu J, Yan X, Ge X, et al. Novel multi-stimuli responsive functionalized PEG-based co-delivery nanovehicles toward sustainable treatments of multidrug resistant tumor. *J Mat Chem B*. 2021;9(5):1297–1314. doi:10.1039/d0tb02192j
26. Kim M, Ahn Y, Lee K, Jung W, Cha C. In situ facile-forming chitosan hydrogels with tunable physicomechanical and tissue adhesive properties by polymer graft architecture. *Carbohydr Polym*. 2020;229115538. doi:10.1016/j.carbpol.2019.115538
27. Fujiwara S, Yoshizaki Y, Kuzuya A, Ohya Y. Temperature-responsive biodegradable injectable polymers with tissue adhesive properties. *Acta Biomater*. 2021;135:318–330. doi:10.1016/j.actbio.2021.08.033
28. Zhou L, Chen F, Hou Z, Chen Y, Luo X. Injectable self-healing CuS nanoparticle complex hydrogels with antibacterial, anti-cancer, and wound healing properties. *Chem Eng J*. 2021;409:128224. doi:10.1016/j.cej.2020.128224
29. Ji G, Zhang Y, Si X, et al. Biopolymer immune implants' sequential activation of innate and adaptive immunity for colorectal cancer postoperative immunotherapy. *Adv Mater*. 2021;33(3). doi:10.1002/adma.202004559.
30. Liu Y, Li T, Sun M, et al. ZIF-8 modified multifunctional injectable photopolymerizable GelMA hydrogel for the treatment of periodontitis. *Acta Biomater*. 2022;146:37–48. doi:10.1016/j.actbio.2022.03.046
31. Si X, Ji G, Ma S, et al. Biodegradable implants combined with immunogenic chemotherapy and immune checkpoint therapy for peritoneal metastatic carcinoma postoperative treatment. *ACS Biomater Sci Eng*. 2020;6(9):5281–5289. doi:10.1021/acsbiomaterials.0c00840
32. Jing X, Xu C, Su W, et al. Photosensitive and conductive hydrogel induced innerved bone regeneration for infected bone defect repair. article. *Adv Healthcare Mater*. 2023;12(3).2370009
33. Motasadizadeh H, Tavakoli M, Damoogh S, et al. Dual drug delivery system of teicoplanin and phenamil based on pH-sensitive silk fibroin/sodium alginate hydrogel scaffold for treating chronic bone infection. *Article Biomaterials Adv*. 2022:139213032. doi:10.1016/j.bioadv.2022.213032
34. Yao F, Wu X, Liao Y, Yan Q, Li Y. Smart chimeric lysin ClyC loaded alginate hydrogel reduces staphylococcus aureus induced bone infection. *Article Frontiers in Materials*. 2021;8763297. doi:10.3389/fmats.2021.763297
35. Boot W, Vogely HC, Nikkels PGJ, et al. PROPHYLAXIS OF IMPLANT-RELATED INFECTIONS BY LOCAL RELEASE OF VANCOMYCIN FROM A HYDROGEL IN RABBITS. article. *Eur Cells Mater*. 2020;39:108–120. doi:10.22203/eCM.v039a07
36. Song Y, Hu Q, Liu Q, Liu S, Wang Y, Zhang H. Design and fabrication of drug-loaded alginate/hydroxyapatite/collagen composite scaffolds for repairing infected bone defects. Article. *J Mater Sci*. 2023;58(2):911–926. doi:10.1007/s10853-022-08053-3
37. Li Y, Liu X, Li B, et al. Near-infrared light triggered phototherapy and immunotherapy for elimination of methicillin-resistant staphylococcus aureus biofilm infection on bone implant. article. *Acs Nano*. 2020;14(7):8157–8170. doi:10.1021/acsnano.0c01486
38. Santos JHPM, Oliveira CA, Rocha BM, Carretero G, Rangel-Yagui CO. Pegylated catalase as a potential alternative to treat vitiligo and UV induced skin damage. *Bioorg Med Chem*. 2021;30115933. doi:10.1016/j.bmc.2020.115933
39. Dahlan NA, Teow SY, Lim YY, Pushpamalar J. Modulating carboxymethylcellulose-based hydrogels with superior mechanical and rheological properties for future biomedical applications. *Express Polym Lett*. 2021;15(7):612–625. doi:10.3144/expresspolymlett.2021.52
40. Yang G, Li Y, Zhang S, et al. Double-cross-linked hydrogel with long-lasting underwater adhesion: enhancement of maxillofacial in situ and onlay bone retention. article. *ACS Appl Mater Interfaces*. 2023;15(40):46639–46654. doi:10.1021/acsami.3c09117
41. Amiryaghoubi N, Fathi M, Safary A, Javadzadeh Y, Omidi Y. In situ forming alginate/gelatin hydrogel scaffold through schiff base reaction embedded with curcumin-loaded chitosan microspheres for bone tissue regeneration article. *Int J Biol Macromol*. 2024;256128335. doi:10.1016/j.ijbiomac.2023.128335
42. Padrao T, Dias J, Carvalho A, Pinto MT, Monteiro FJ, Sousa SR. Vancomycin-loaded bone substitute as a ready-to-use drug delivery system to treat osteomyelitis article. *Ceram Int*. 2023;49(15):24771–24782. doi:10.1016/j.ceramint.2023.04.239
43. Xiao S, Yuan L, Liu J, et al. Vancomycin-loaded silica coatings for controlled release of drug and si ions to repair infected bone defects. article. *Surf Coat Technol*. 2023:463129525. doi:10.1016/j.surfcoat.2023.129525
44. Solanki T, Maurya MK, Singh PK. Results of antibiotic-impregnated cement/polymer-coated intramedullary nails in the management of infected nonunion and open fractures of long bones. *Cureus J Med Science*. 2023;15(8).
45. Mills AG, Dupper AC, Chacko KI, et al. Methicillin-resistant staphylococcus aureus bacteremia with elevated vancomycin minimum inhibitory concentrations. *Antimicrobial Stewardship & Healthcare Epidemiology*. 2023;3(1).e87
46. Kavarthapu V, Giddie J, Kommalapati V, Casey J, Bates M, Vas P. Evaluation of adjuvant antibiotic loaded injectable bio-composite material in diabetic foot osteomyelitis and charcot foot reconstruction. article. *J Clin Med*. 2023;12(9):3239. doi:10.3390/jcm12093239
47. Jung SW, Oh SH, Lee IS, Byun J-H, Lee JH. In situ gelling hydrogel with anti-bacterial activity and bone healing property for treatment of osteomyelitis. *Tissue Eng and Regener Med*. 2019;16(5):479–490. doi:10.1007/s13770-019-00206-x
48. Yoeruek E, Spitzer MS, Saygili O, et al. Comparison of in vitro safety profiles of vancomycin and cefuroxime on human corneal endothelial cells for intracameral use article. *J Cataract Refract Surg*. 2008;34(12):2139–2145. doi:10.1016/j.jcrs.2008.08.022

49. Petit C, Batool F, Stutz C, et al. Development of a thermosensitive statin loaded chitosan-based hydrogel bone article. *Int J Pharm*. 2020:586119534. doi:10.1016/j.ijpharm.2020.119534
50. Demeter M, Meltzer V, Calina I, Scarisoreanu A, Micutz M, Kaya MGA. Highly elastic superabsorbent collagen/PVP/PAA/PEO hydrogels crosslinked via e-beam radiation article. *Radiat Phys Chem*. 2020;174108898. doi:10.1016/j.radphyschem.2020.108898
51. Liang J, Li J, Zhou C, et al. In situ synthesis of biocompatible imidazolium salt hydrogels with antimicrobial activity. *Acta Biomater*. 2019;99:133–140. doi:10.1016/j.actbio.2019.09.020
52. Fourie J, Taute F, du Preez L, de Beer D. Novel chitosan-poly(vinyl acetate) biomaterial suitable for additive manufacturing and bone tissue engineering applications. *J Bioact Compat Polym*. 2021;36(5):394–413. 08839115211043279. doi:10.1177/08839115211043279
53. Chen M, Li Y, Hou W-X, Peng D-Y, Li JK, Zhang H-X. The antibacterial effect, biocompatibility, and osteogenesis of vancomycin-nanodiamond composite scaffold for infected bone defects. article. *Int J Nanomed*. 2023;18:1365–1380. doi:10.2147/ijn.S397316
54. Russell AD, Thomas IL. Effect of mg on the activity of vancomycin against escherichia coli. *Appl Microbiol*. 1966;14(6):902–904. doi:10.1128/am.14.6.902-904.1966
55. Yu C, Chen L, Zhou W, et al. Injectable bacteria-sensitive hydrogel promotes repair of infected fractures via sustained release of mirna antagonist. article. *ACS Appl Mater Interfaces*. 2022;14(30):34427–34442. doi:10.1021/acsami.2c08491
56. Xu L, Ye Q, Xie J, et al. An injectable gellan gum-based hydrogel that inhibits staphylococcus aureus for infected bone defect repair. article. *J Mat Chem B*. 2022;10(2):282–292. doi:10.1039/d1tb02230j
57. Zhang Q, Zhou X, Du H, et al. Bifunctional hydrogel-integrated 3D printed scaffold for repairing infected bone defects. article; early access. *ACS Biomater Sci Eng*. 2023. doi:10.1021/acsbiomaterials.3c00564
58. Qian H, Lei T, Hua L, et al. Fabrication, bacteriostasis and osteointegration properties researches of the additively-manufactured porous tantalum scaffolds loading vancomycin. *Article Bioact Mater*. 2023;24:450–462. doi:10.1016/j.bioactmat.2022.12.013
59. Jian G, Li D, Ying Q, et al. Dual photo-enhanced interpenetrating network hydrogel with biophysical and biochemical signals for infected bone defect healing. article; early access. *Adv Healthcare Mater*. 2023. doi:10.1002/adhm.202300469
60. Gao X, Xu Z, Li S, et al. Chitosan-vancomycin hydrogel incorporated bone repair scaffold based on staggered orthogonal structure: a viable dually controlled drug delivery system. article. *RSC Adv*. 2023;13(6):3759–3765. doi:10.1039/d2ra07828g
61. Ren X, Hu Y, Chang L, Xu S, Mei X, Chen Z. Electrospinning of antibacterial and anti-inflammatory Ag@hesperidin core-shell nanoparticles into nanofibers used for promoting infected wound healing. *Regen Biomater*. 2022;9rbac012. doi:10.1093/rb/rbac012